Flow Field Phenomena about Lift and Downforce Generating Cambered Aerofoils in Ground Effect

J.W. VOGT, T.J. BARBER and E. LEONARDI
School of Mechanical and Manufacturing Engineering
The University of New South Wales
Sydney, NSW 2052
AUSTRALIA
j.vogt@student.unsw.edu.au

Abstract: – A Computational Fluid Dynamics investigation was conducted to ascertain and highlight the different ways in which ground effect phenomena are present around both an upright (lift generating) and inverted (downforce generating) cambered aerofoil when in close proximity to the ground. The trends in force and flow field behaviour were observed at various ground clearances, while the angle of attack was held constant at 6 degrees. The different mechanisms by which ground effect influences the two different configurations were highlighted through observation of the pressure coefficient plots, contour maps of velocity and turbulence intensity and their effect on the normal and drag forces. The primary contributing factor to the increase in normal force for the lifting aerofoil, as the ground was approached, was a constriction and rise in pressure of the flow. For the downforce aerofoil, a significantly sped up flow increased suction and enhanced downforce. Also discussed is the observation of a reduction in lift for the upright aerofoil as its ground clearance is reduced through high and medium clearances.

Key-Words: – Aerodynamics, Ground Effect, Computational Fluid Dynamics, Aerofoil

1 Introduction

Over the last 20 years, research interest in the various flow phenomena associated with bodies in close proximity to the ground, has been growing. The aerodynamic behaviour of such bodies is distinctly different from that which would be seen about the body if it were placed far from the ground. These distinct flow characteristics are generically referred to as 'ground effect'.

When the benefits of ground effect are mentioned in relation to race cars, it is often done so in the same breath as references to aeronautical industry, or positive lift producing, applications [13,15]. This generalisation of the influence that the proximity of the ground has on bodies can often be misinterpreted as a consistent process that, more or less, has the same effect on bodies near the ground, regardless of their geometric shape. Ground effect is, therefore, often considered to make a wing (regardless of its orientation) simply work harder, or better. This paper will demonstrate, however, that this is an incorrect and simplistic assertion as the influence ground effect has on upright and inverted aerofoils, is distinctly different.

Various studies have been undertaken in the past to examine and explain the effect of ground effect on upright (lift generating) wings or aerofoils, through analytical, numerical and experimental methods [1,2,4,5,10,12]. Additionally, various studies have sought to explain ground effect about inverted (downforce generating) wings or aerofoils, mainly through numerical and experimental means [3,6,7,8,11,16,17].

The aforementioned studies have considered either an upright aircraft style wing or aerofoil or an inverted racing car style wing or aerofoil. However, no researcher has sought to clarify the differences between ground effect phenomena for upright and for inverted aerofoils. That is the primary aim of this study.

A two-dimensional Computational Fluid Dynamics (CFD) study, using a steady Reynolds-Averaged Navier-Stokes (RANS) solver, was undertaken to examine ground effect about a cambered aerofoil in both the upright and inverted position. The study was conducted at a representative Reynolds number, Re, of 458,800. The aerofoil was placed at a constant angle of attack of 6º and its height above the ground was varied. The investigation is restricted to the two-dimensional case in order to clarify the fundamental flow phenomena without the added complexity of wing-tip vortices and other three-dimensional effects. The aerofoil modelled is the Tyrrell aerofoil which, in its original inverted form, was the cross-section of the main-plane of the 1998 Tyrrell

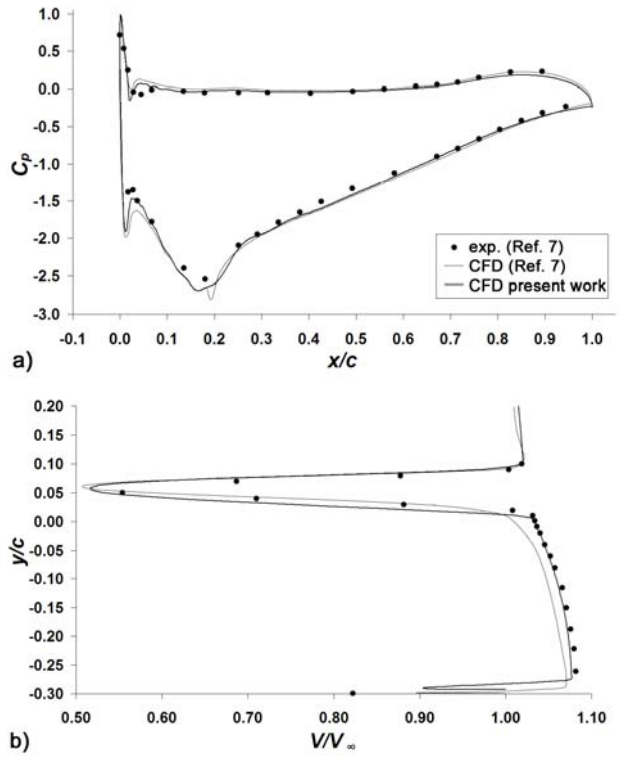

Fig 1. Validation case; (a) pressure coefficient plot for h/c = 0.224, (b) velocity deficit in wake flow at x/c = 1.2.

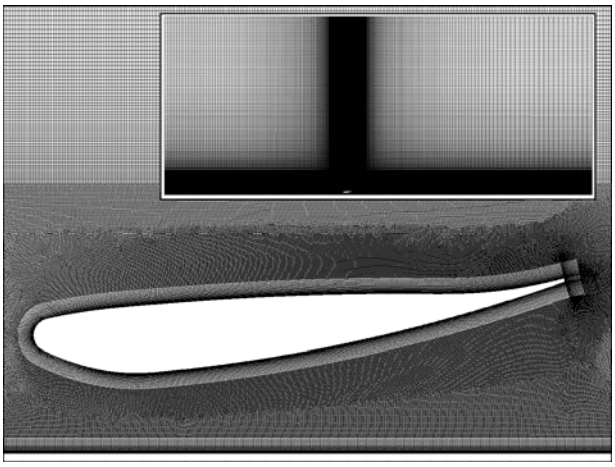

Fig 2. Mesh structure about inverted aerofoil, h/c = 0.15, α = 6° (inset) entire domain mesh.

Formula 1 racing car [14]. Of primary interest in this investigation are the pressure-coefficient plots and flow-field results in the immediate vicinity of the aerofoil.

2 Numerical Model

The demands of this study required the construction of five models listed here in order of construction: 1) a validation model, simulating the spanwise mid-plane of the wind tunnel of Mahon and Zhang [7], in order to validate against their experimental and numerical C_p and wake data; 2) a ground effect model, similar to model (1), featuring a moving ground and open air condition; 3) a second validation model based on model (2) but adapted to validate against experimental C_n and C_d results from Ahmed et al [1]; 4) a 'freestream' model to simulate the out-of-ground condition and, finally; 5) a third validation model, based on (4), to validate against experimental freestream C_p and C_n results from Pinkerton [9].

These various models and the numerical methods employed are discussed briefly below.

2.1 Validation Models

A full discussion of the validation models cannot be included here, however, will be available in a future publication by the same authors, currently under review for inclusion in a leading journal.

In summary, validation model (1) achieved a very good match to the experimental data, as shown in Figure 1. Validation model (2) achieved reasonable agreement with its comparison case and validation model (3) achieved very close agreement with its comparison case.

2.2 Ground Effect Model

The ground effect model grid was constructed of three primary elements: a structured boundary layer around the surface of the aerofoil and the ground, consisting of 20 rows of expanding thickness with a total height of 0.03c (normal to the boundary surface); a rectangular box surrounding the aerofoil and containing unstructured triangular cells and the remainder of the domain was composed of structured quadrilateral cells. The unstructured section of the mesh was designed as such to maximise the ease with which the mesh could be adapted when changing the clearance of the aerofoil in later simulations. The mesh was designed to concentrate the cells around the aerofoil and also near the ground. The mesh was designed to simulate an open air condition. The aerofoil was tested in both its upright and inverted configuration and was set at an angle of α = +6º to the horizontal in both cases. Additionally, both aerofoil configurations were simulated at the following ground clearances: h/c = 3.00, 2.00, 1.50, 1.00, 0.75, 0.50, 0.40, 0.30, 0.20 and 0.15. The upright aerofoil was simulated at the additional ground clearances of h/c = 0.10, 0.05 and 0.03. Lack of numerical stability, brought on by inherent unsteadiness in the flow, prevented the inverted aerofoil simulations from converging at these additional very low clearances. It was decided

that modelling inherently unsteady flow about this aerofoil was beyond the scope of this work.

To achieve adequate grid boundary independence, the inlet, outlet and upper boundary were positioned at +15*c*, +20*c* and +15*c* from the aerofoil, respectively. The upper boundary was designated a symmetry plane which specified no fluxes (of any variable) across the top boundary, thus ensuring a horizontal vector field at the upper boundary. For the various ground clearances modelled, the ground plane was moved further below the aerofoil to accommodate the increase in ground clearances between h/c = 0.03 and 3.00. The TI value was set to 0.1% at the inlet and the freestream velocity was set to 30m/s.

The boundary independence of this model was assessed by testing a model with all its boundaries (except the ground) extended by a further 5 chord lengths away from the aerofoil (inlet +20*c*, outlet +25*c* and upper boundary +20*c*). In comparison to this extended boundary case, the standard model, with the aerofoil positioned at h/c = 0.20, saw an insignificant 0.034% increase in C_n and a 0.051% increase in C_d. The standard model was thus deemed sufficiently boundary independent.

Grid convergence was assessed by constructing two grids with varying refinement that are otherwise identical to the baseline case; a coarse grid with approximately half the number of cells of the baseline case at 184,000, down from 365,000; and a fine grid with roughly double the cells of the baseline case at 682,000. The coarse grid generated C_n and C_d values that were in very close agreement with the standard mesh. The C_n value for the coarse mesh exceeded that of the standard mesh by 1.052% and the C_d exceed the standard mesh value by only 0.112%. The fine mesh presented very similar results with the C_n value exceeding the baseline case by only 0.014% and the C_d value also exceeding the baseline case by 0.078%. These consistent results indicated that the performance of the simulation varied little with changing grid fineness. Despite achieving good agreement with even the coarse grid, and as it was feasible to do so with the resources available, the baseline grid was retained for the remainder of the investigation in an effort to more accurately resolve the flow features of the more extreme geometries under investigation (low h/c cases).

The mesh size ranges from 246,000 cells at h/c = 0.03 to 854,000 cells at h/c = 3.00. This large increase is due to the high concentration of cells in the additional space under the aerofoil (and also upstream and downstream of this location) at higher clearances. The concentration of cells in the boundary layer remained constant. A typical mesh, in the immediate vicinity of the aerofoil, is shown in Figure 2.

2.3 Out of Ground Model

The out-of-ground or freestream model was built as a comparison case against which to compare the ground effect data. This model is essentially the same as the ground effect model except the domain area is doubled by mirroring the ground effect model's mesh structure about the ground plane (which is no longer defined as a boundary, in this case as it now defines the middle of the domain). The aerofoil remains in essentially the same position which after mirroring the mesh, is now located in the middle of the domain. The new lower boundary, like the upper boundary, is thus defined as a symmetry plane and is located approximately 15*c* below the aerofoil. The final mesh has 653,000 cells.

2.4 Numerical Solver

All simulations were conducted using an implicit, steady, RANS solver. The QUICK discretisation scheme was used for all flow variables and turbulent quantities in order to best minimise numerical diffusion. The SIMPLEC pressure-velocity coupling was employed for all cases, as was the RSM turbulent closure model.

The simulation was stopped when convergence was considered achieved for both the C_n and C_d values. The normal force and drag force coefficients, C_n and C_d, were considered converged when plots of these quantities (with iterations on the ordinate) levelled out such that their variation per iteration was consistently below 0.01%.

The applicability of this numerical model is limited to steady-state cases and, as such, not all ground clearances could be computed while maintaining a steady flow solution.

3 Results and Discussion

3.1 Force Behaviour

The normal force is defined as the component of generated force that acts perpendicular to the direction of travel of the aerofoil (or in a wind tunnel context, the direction of travel of the freestream air). The sense of this force vector is considered positive under normal operation of the given aerofoil configuration. It is convenient to consider the force behaviour of both aerofoil

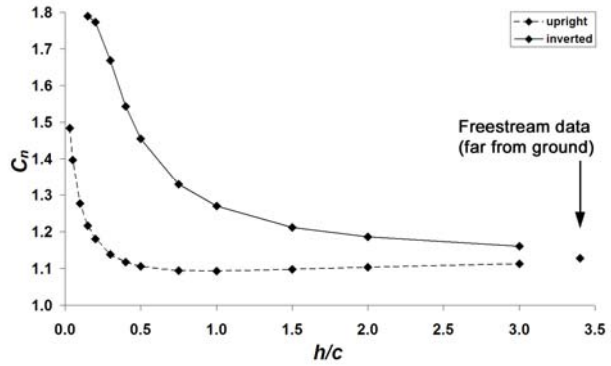

Fig 3. Coefficient of normal force (C_n) vs. ground clearance.

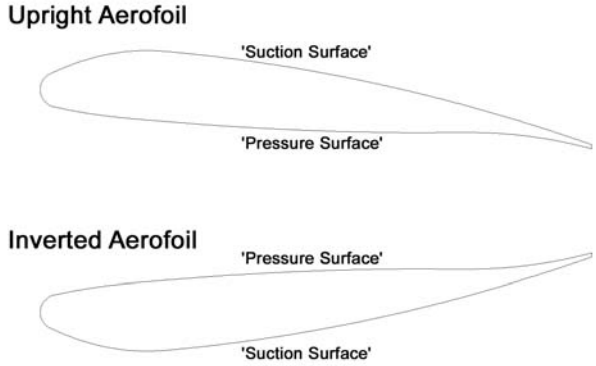

Fig 4. Adopted aerofoil surface name convention.

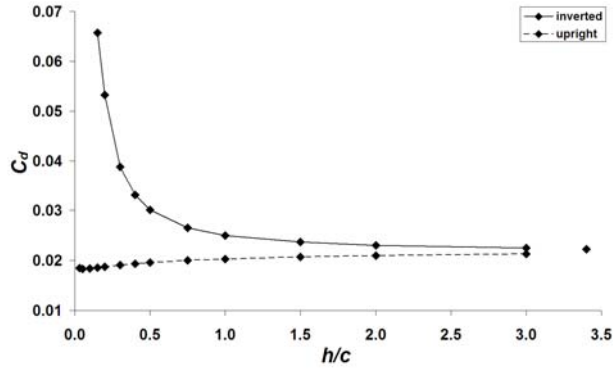

Fig 5. Coefficient of drag (C_d) vs. ground clearance.

configurations in terms of the normal force, n, as the performance of both aerofoils can then be directly compared despite the lift vector of each aerofoil pointing in the opposite direction to that of the other.

The normal force coefficient, C_n, for both the upright and inverted Tyrrell aerofoils, over their applicable ground clearance ranges, is shown in Figure 3. The freestream result is also plotted on this Figure (as a discontinuous data point). Both aerofoils exhibit a fairly dramatic increase in C_n at low ground clearances with the upright aerofoil achieving a maximum 31.6% increase in C_n in comparison to its freestream performance and the inverted aerofoil achieving a significantly greater 58.6% increase. It should be noted that both these maximum C_n readings may not represent the true maximums possible as the test cases did not extend all the way to the ground. However, it is likely the curves would not extend very much higher with any further decrease in h/c as is it well established that both upright and inverted aerofoils experience a force reduction region at extremely low ground clearances [5, 16]. In fact, the onset of such a region is visible in the lessening slope of the inverted aerofoil curve at h/c = 0.15.

For each aerofoil, the highly cambered side which features accelerated flow (and associated suction force) is called the 'suction side' of the aerofoil. This corresponds to the bottom side of the inverted aerofoil and the top side of the upright aerofoil. The other, less cambered side features slower flow and, usually, a positive pressure force. This side is called the 'pressure side' and is the top side of the inverted aerofoil and the bottom side of the upright aerofoil. These terms will be used hereafter and are presented graphically in Figure 4.

The drag force coefficient, C_d, was determined for each aerofoil ground clearance and configuration and is presented in Figure 5. The difference in performance is very stark with the C_d of the inverted aerofoil increasing slowly at high clearances and then very dramatically at low and very low clearances. The C_d trend of the upright aerofoil, however, progressively decreases slightly all the way down to h/c = 0.05 and then increases very slightly at the lowest clearance of h/c = 0.03. The upright aerofoil's C_d decreases by a maximum of 17.53%, compared to freestream, at h/c = 0.05 and the inverted aerofoil's C_d increases by a maximum of 195.99% at h/c = 0.15. Despite this considerable drag increase for the inverted case, a further reduction in ground clearance (below clearances simulated here) would result in even higher levels of drag [16].

3.2 Pressure Coefficient Distribution

Plots of the pressure coefficient, C_p, distribution over both aerofoils were recorded for all cases. The C_p distributions, at selected clearances, for the inverted aerofoil are shown in Figure 6. A characteristic of the Tyrrell aerofoil, are the relatively sharp curves on both the pressure and suction surfaces, near the leading edge. As can be seen in Figure 6, these sharp curves result in a localised sudden decrease in pressure as the flow speeds up around these corners. These features are referred to as the pressure and suction surface 'suction spikes'. In freestream, the aerofoil features a fairly constant positive pressure along the pressure

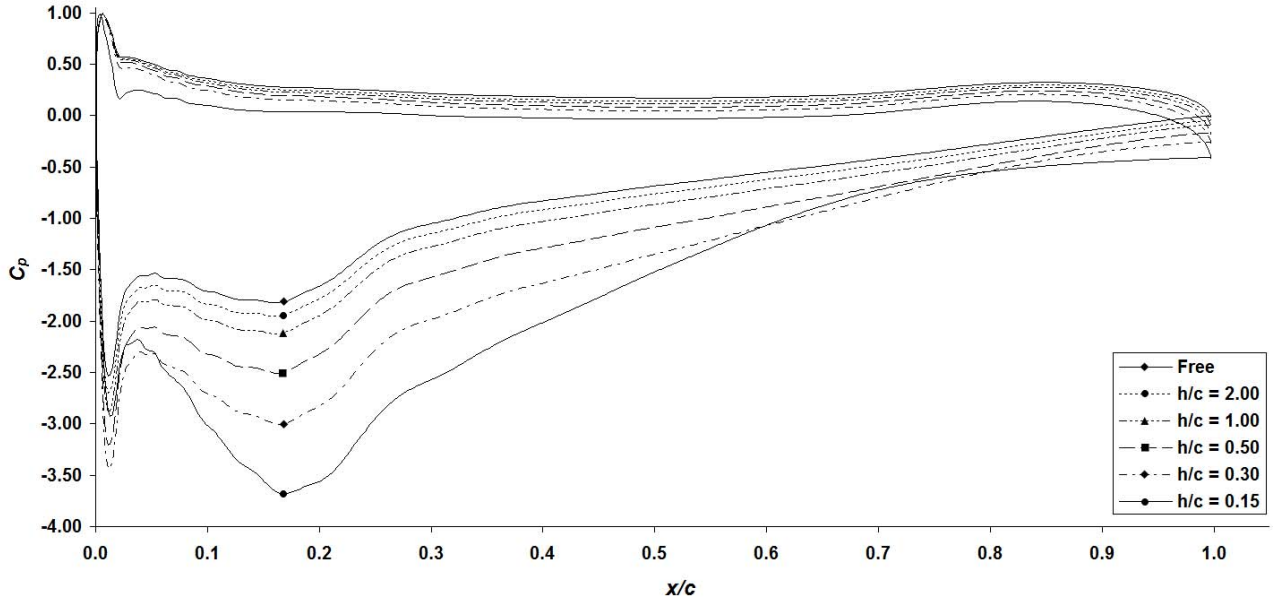

Fig 6. Pressure coefficient distributions for inverted aerofoil at various ground clearances.

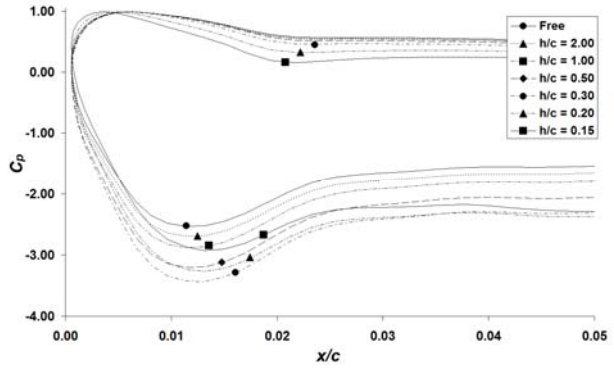

Fig 7. Leading edge region from Figure 6 about inverted aerofoil.

surface and, after the maximum suction point on the suction surface, at approximately x/c = 0.15, a long adverse pressure gradient region.

As the inverted aerofoil is brought closer to the ground, the suction is increased over the suction surface, particularly in the maximum suction region of x/c = 0.1–0.2. This increased suction results in an increased pressure recovery demand. The pressure is also consistently, but only slightly, decreased over the whole pressure surface, as h/c is reduced. Below h/c = 0.75 (not shown in the Figure), the suction strength, on the bottom surface, and the accompanying adverse pressure gradient, begin to increase dramatically, eventually resulting in a severe adverse pressure gradient and the onset of flow separation at h/c = 0.15. As shown in the close-up of the leading edge region, in Figure 7, decreasing clearance also strengthened the suction spike, on the suction surface, down to h/c = 0.3, below which, the suction spike started to decrease in strength. Below this same clearance, the pressure surface suction spike begins to noticeably increase in strength.

Figure 8 shows the C_p plots for the upright aerofoil. As h/c is reduced, a consistent but slight, increase in pressure can be seen on both the suction and pressure surfaces down to a clearance of h/c = 0.75 (not shown). Below this height, the pressure over the suction surface continues to increase slightly, with no appreciable change to the adverse pressure gradient, however, the pressure on the pressure surface (surface facing the ground for this aerofoil) starts to increase rapidly. Below h/c = 0.15, the suction spike on the suction surface, having decreased in strength down to this height, starts markedly gaining strength, see the close-up of the leading edge region in Figure 9. The suction spike on the pressure surface is continually weakened with decreasing h/c as the pressure continues to increase on that surface.

The pressure coefficient plots reinforce very clearly that the flow behaviour is altered about the inverted and upright aerofoils in distinctly different ways when brought into close proximity to the ground. The very large increase in suction seen under the inverted aerofoil is essentially the sole contributor to the aerofoil's increase in C_n at low h/c. The contribution from the pressure surface all but disappears as the pressure over this surface reduces to approximately the freestream static value by h/c = 0.15. The increase in adverse pressure gradient is clear to see from Figure 6 and its effect to increase the boundary layer thickness and increase TI is clearly evident from plots of velocity contours and TI (Figures 10(a-c) and 11(a)).

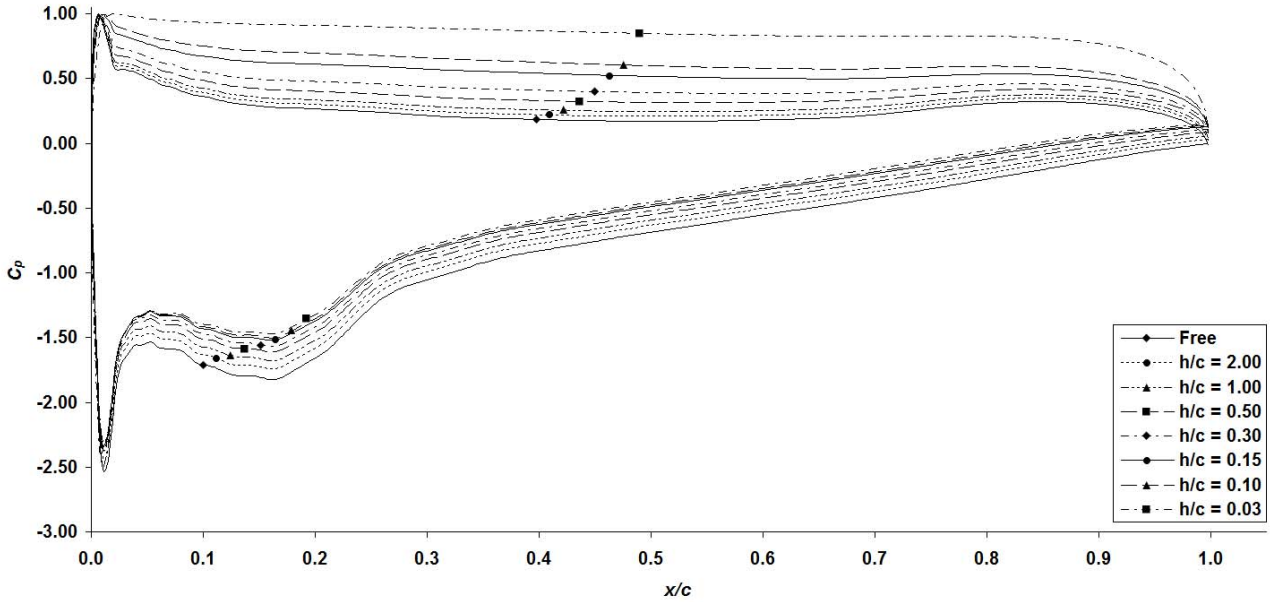

Fig 8. Pressure coefficient distributions for upright aerofoil at various ground clearances.

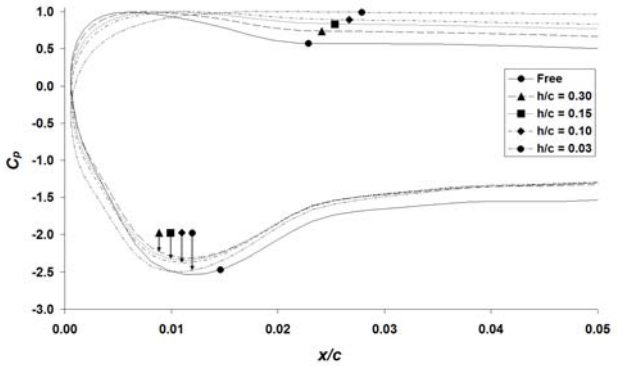

Fig 9. Leading edge region from Figure 8 about upright aerofoil.

Velocity contours and TI plots will be discussed in detail later.

The adverse pressure gradient on the suction surface of the upright aerofoil remains predominantly unchanged and the result of this can be seen in the far thinner and less turbulent boundary layer (Figures 10(d-f) and 11(b)). As apposed to the inverted aerofoil case, both sides of the upright aerofoil continue to contribute significantly to C_n down to very low *h/c*. The speed of the flow over the suction surface does decrease, hence the increase in pressure on the C_p plots, however, even at it lowest contribution, the suction surface still produces 40.8% of total C_n at *h/c* = 0.03.

3.3 Velocity Contours

Velocity contour maps were observed for all cases and a selection is presented in Figure 10. Figures 10(a-c) show the change in the velocity field around the inverted aerofoil as it approaches the ground through *h/c* = 1.00, 0.30 and 0.15, respectively. It can be seen that at *h/c* = 1.00, the boundary layer on the suction side of the aerofoil is still relatively thin, though turbulent, beyond about *x/c* = 0.20, and the wake is not yet significant. The turbulent nature of the flow is evident from the sudden increase in the rate of boundary layer growth at *x/c* = 0.20. However, as the aerofoil is brought down to *h/c* = 0.30, Figure 10(b), the boundary layer thickness has increased significantly on the suction side feeding into a, now, quite large wake region. At this height, the region between the aerofoil and the ground, now forming a distinct diffuser shape, features a fast moving flow through the throat section which, with an average speed of 52.3 m/s through the throat – up from 40.3 m/s at *h/c* = 1.00. Beyond the throat, the flow then starts to reduce in speed down to that approaching freestream near the trailing edge. At the lowest point considered in this investigation, *h/c* = 0.15, Figure 10(c), the boundary layer now spans about one-third of the distance to the ground at the trailing edge and the wake is even thicker. The flow through the throat region is now moving extremely quickly with its average speed now 60.49 m/s which is more than double the freestream speed.

Throughout the clearance range down to the ground, the velocity field about the pressure side of the aerofoil remains quite consistent with minimal change in overall velocity and boundary layer thickness. Additionally, although the boundary layer on the suction surface grows significantly with reduced clearance, it always remains extremely thin until back to the throat section (*x/c* < 0.2).

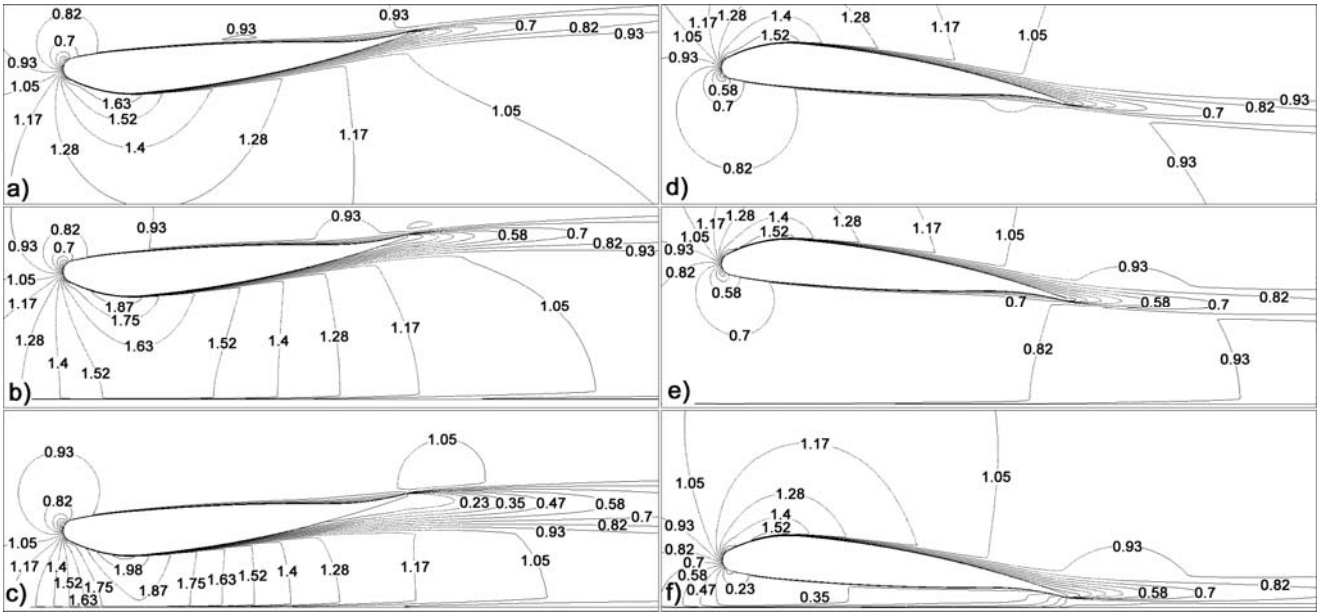

Fig 10. Velocity contours (V/V_∞) about inverted aerofoil at; (a) h/c = 1.00, (b) h/c = 0.30 and (c) h/c = 0.15, and upright aerofoil at; (d) h/c = 1.00, (e) h/c = 0.30 and (f) h/c = 0.03.

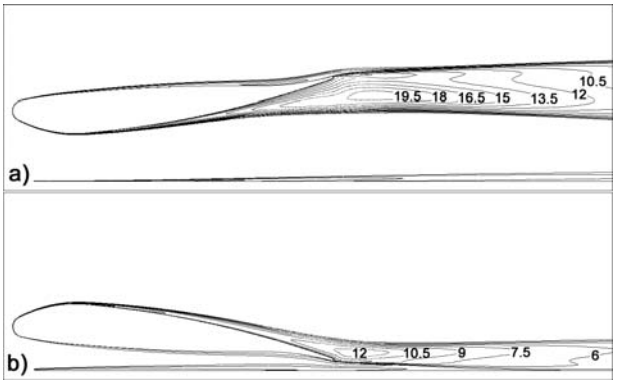

Fig 11. Contours of turbulence intensity percentage; (a) inverted aerofoil at h/c = 0.15, (b) upright aerofoil at h/c = 0.03.

Figures 10(d-f) show the variation of the velocity contours around the upright wing for ground clearances of h/c = 1.00, 0.30 and 0.03, respectively. At h/c = 1.00, the boundary layer on the suction surface (upper surface) is still relatively thin, leading to a fairly small wake. This is very similar to the suction surface of the inverted wing at this same clearance. The speed of the flow over the top of the aerofoil is slightly reduced in comparison to the freestream case, which is not shown here. The boundary layer on the suction surface increases in thickness only marginally as the aerofoil is brought down to h/c = 0.30, see Figure 10(e). This leads to a slightly thicker wake region. The speed of the flow over the top of the wing is clearly reduced in comparison to the h/c = 1.00 case. At the lowest clearance of h/c = 0.03, Figure 10(f), The suction surface boundary layer has grown further, leading again to a slightly larger wake region, but the boundary layer growth is insignificant in comparison to that of the inverted aerofoil, whose size down to h/c = 0.15 (still 0.12c higher than this case) is significantly larger in comparison.

The variation in the flow field about the pressure surface of the upright aerofoil, as it approaches the ground, is of primary interest for this aerofoil as the variation about the suction surface is fairly minimal. At h/c = 1.00, Figure 10(d), the velocity field around the pressure surface is starting to be impeded and, with no adverse pressure gradient, the boundary layer remains very thin all the way to the trailing edge. By the time the aerofoil reaches h/c = 0.30, Figure 10(e), the nozzle effect formed between the pressure surface of the aerofoil and the ground is now clearly apparent. Consequently, the flow is starting to be slowed toward the front of the nozzle section and is being 'squeezed' out the rear at a speed approaching (but still below) freestream. Between h/c = 1.00 and h/c = 0.30, the average velocity between the trailing edge and the ground has reduced from 26.86 m/s to 25.48 m/s, respectively. However, the nozzle flow is now quicker in comparison to the flow nearer the leading edge, indicating a more significant reduction in average speed toward the front of the aerofoil. The boundary layer remains very thin. Finally, at h/c = 0.03, Figure 10(f), the nozzle effect is now very strong with the flow speed at the entrance to the nozzle highly restricted by the limitations imposed on the mass flow rate out the rear of the section. The average speed of the flow through the nozzle is now 25.35 m/s, but with the nozzle so small, the flow toward the front of the aerofoil is comparatively very slow, varying between 0.0–13.0 m/s (down

from an original freestream value of 30m/s) for most of the length of the nozzle section.

3.4 Turbulence Intensity

To examine the level of turbulence in the flow, TI values about the inverted and upright aerofoils are presented in Figure 11(a) and 11(b), respectively, at their lowest ground clearances. The inverted aerofoil case shows a significant development of turbulence within the suction surface boundary layer, downstream of the throat, and a highly turbulent wake. The pressure surface, however, shows a far lower level of turbulence within its boundary layer. The maximum TI value for the inverted aerofoil was 20.34% in the near wake and the maximum wall TI value was 19.42% at the suction spike on the suction surface.

The TI values around the upright aerofoil, in Figure 11(b), indicate an overall lower level of turbulence intensity with the maximum value within the boundary layer or wake region about 13.3%, 34% lower than that of the inverted aerofoil. The maximum TI value appeared on the aerofoil surface, again at the suction surface suction spike and its value was 18.18%, down slightly on the inverted case. The pressure surface, like the inverted case, showed only marginal turbulent growth. The suction surface shows a much higher turbulent growth within the boundary layer, in comparison to the pressure side, but this is still insignificant when compared to the suction surface turbulent growth on the inverted case.

3.5 Dividing Streamlines and Effect on Aerodynamic Behaviour

An effort was made to observe the trends in the behaviour of the close range flow upstream and downstream of both aerofoils. The dividing streamline terminates at the stagnation point at the leading edge and effectively divides the flow into that going over the aerofoil and that going under it. Similarly, the dividing streamline downstream emanates from the trailing edge and divides the flow into that which went over and that which went under the aerofoil. The position of the dividing streamline, relative to the leading edge of the aerofoil, was recorded three chord lengths upstream and downstream of the aerofoil. This is demonstrated graphically in Figure 12, and the results are presented in Figure 13. The dividing streamline for the inverted aerofoil moves slowly downward, toward the leading edge, as the aerofoil approaches

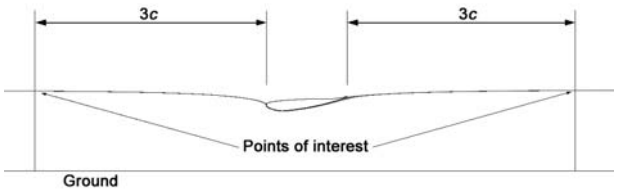

Fig 12. Dividing streamlines on inverted aerofoil at h/c = 1.00, α = 6º.

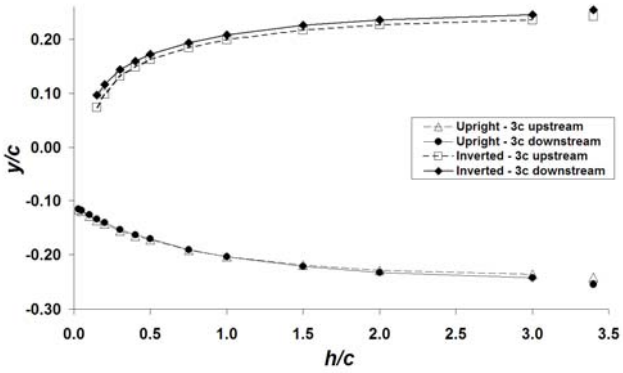

Fig 13. Position of dividing streamline at 3 chords distance from aerofoils vs. ground clearance.

the ground. As the aerofoil nears the ground this downward movement becomes much more pronounced. The upstream dividing streamline is consistently lower than its downstream counterpart and the gap between them remains fairly constant over the clearance range. The streamlines' position changes from y/c = 0.242–0.255 in freestream down to y/c = 0.074–0.097 at h/c = 0.15.

The upright aerofoil case demonstrates a similar but opposite trend as the streamlines initiate below the leading edge at freestream (as this is a mirror image of the inverted case) and then trend up toward the leading edge as h/c is reduced. In contrast to the inverted case, the streamline movement is not as pronounced as the inverted case with the overall movement less than the inverted case, even including the upright case's larger range of h/c. Additionally, the downstream dividing streamline, which sits further down than the upstream one at freestream, eventually crosses over the upstream trend between h/c = 0.75–1.00. Below this height, it remains slightly above the upstream trend.

As mentioned earlier, the upright aerofoil experiences a decrease in C_n as ground clearance is reduced from freestream down to about h/c = 1.00. This behaviour was unexpected, although a similar phenomenon has previously been observed by Coulliette and Plotkin [4] about a cambered arc using a discrete vortex method. A close inspection of the C_p plots, about the upright aerofoil (Figures 8 and 9), indicate that for h/c down to 1.00, the pressure on the pressure surface does not increase significantly in comparison to the increase at lower

clearances, however, the increase in pressure on the suction surface is far more comparable to that seen at lower clearances. This suggests that at high and medium clearances, before the effect of the increased pressure under the wing becomes predominant, a general reduction in circulation about the aerofoil causes it to decrease in C_n throughout this height range. The slower flow over the suction surface, and associated lift losses, is more significant in this height range than the marginal increase in pressure seen on the pressure surface.

A potential reason for the decrease in circulation about the upright wing is a gradual decrease in the effective angle of attack as ground clearance is reduced. This can be seen through the trends of the dividing streamlines. In the freestream condition, the dividing streamlines, three chords upstream and downstream of the aerofoil, are located at $y/c = -0.24$ and -0.25, respectively. A rough estimate of the effective change in angle of attack due to the oncoming flow direction, $\Delta\alpha$, may be considered the angle of the flow from this dividing streamline position to the leading edge, which in this case is approximately 4.6º. This additional incidence angle will result in a higher C_n value than if the incident flow vector was merely horizontal. The wake flow behind the aerofoil exhibits similar behaviour, as mentioned above, with the flow heading downward at a similarly estimated angle of 4.8º. In this two-dimensional aerofoil case, the angle of the wake flow can not be considered downwash due to tip vortices, as three dimensional effects have not been considered in this CFD analysis. Rather, it is likely the result of momentum considerations with the aerofoil acting much like a turning vane, deflecting the flow further for a given increase in the effective angle of attack.

As the aerofoil is brought closer to the ground, the effective angle of attack, $\alpha_{eff} = \alpha + \Delta\alpha$, reduces due to a continual reduction in $\Delta\alpha$. This reduction is caused by the upward movement (relative to the aerofoil) of the dividing streamline in front of the aerofoil resulting in a smaller $\Delta\alpha$. With a reduced effective angle of attack, the aerofoil sees less circulation and produces less lift and drag. Additionally, the deflection of the flow in the wake reduces in kind. At low clearances, $\Delta\alpha$ continues to diminish toward zero and thus becomes insignificant in comparison to the now dominant effects seen at low clearances – namely the nozzle effect that stifles the flow under the aerofoil.

A similar phenomenon can be seen about the inverted aerofoil, however, its C_n value does not reduce as clearance is reduced through medium clearances, as seen on the upright aerofoil. This would appear to be the case because the negative (or non-productive) effect of the reduction in effective angle of attack is outweighed by the positive effect of the diffuser which starts to noticeably influence the C_n value of the aerofoil far earlier than the nozzle effect does for the upright aerofoil. This is evident by observation of the C_p plots which show an immediate and tangible increase is suction under the inverted aerofoil as clearance is initially reduced from freestream and is contrasted by the lack of significant change in the pressure on the pressure side of the upright aerofoil until below $h/c = 1.00$.

4 Conclusions

A numerical simulation of the flow about both an upright and inverted Tyrrell aerofoil at various ground clearances was undertaken to ascertain and highlight the differences in the 'ground effect' phenomena seen about these aerofoils. The following primary conclusions may be drawn from this investigation:

(1) The only significant contributor to the increase in downforce seen for the inverted aerofoil was the increase in suction under the aerofoil. Any contribution from the pressure side of the aerofoil diminished in close proximity to the ground. In contrast, the increase in lift seen on the upright aerofoil, when close to the ground, was a combination of a large increase in pressure lift and also, in large part, due to the suction on its upper surface.

(2) The normal force increase was significantly higher for the inverted aerofoil in close ground proximity, however, the drag for the inverted aerofoil also increased significantly compared to a slight decrease for the upright aerofoil.

(3) The upright aerofoil saw a large increase in l/d, from freestream to the ground, while the inverted aerofoil suffered an equally large decrease in l/d. This indicates that operation in ground effect is beneficial for the upright aerofoil, both in terms of outright performance and efficiency. Ground effect operation for the inverted aerofoil is extremely beneficial in terms of outright *Cn* performance, however, its efficiency suffers significantly.

(4) The lift produced by the upright aerofoil slowly diminished down to a clearance of $h/c = 1.00$. This decrease is due to a reduction in the effective angle of attack of the incident air and a consequent reduction in lift. A similar reduction in angle of attack was seen for the inverted aerofoil, however, the beneficial effect of the diffuser formed

between the aerofoil and the ground more than cancelled this negative effect.

References:

[1] Ahmed, M.R., Takasaki, T. & Kohama, Y., Aerodynamics of a NACA4412 Airfoil in Ground Effect, AIAA Journal, Vol. 45, No. 1, January 2007, pp. 37-47.

[2] Ahmed, N.A. & Goonarate, J., Lift Augmentation of a Low-Aspect-Ratio Thick Wing in Ground Effect, Journal of Aircraft, Vol. 39, No. 2, March-April 2002, pp. 381-384.

[3] Beves, C., Barber, T.J. & Leonardi, E., Near-Wake Properties of the Tyrrell-026 Aerofoil in Inverted Ground Effect, 5th Pacific Symposium on Fluid Flow Visualisation and Image Processing, Australia, 27-29 September 2005.

[4] Coulliette, C. & Plotkin, A., Aerofoil Ground Effect Revisited, Aeronautical Journal, February 1996, pp. 65-74.

[5] Hsiun, C. & Chen, C., Aerodynamic Characteristics of a Two-Dimensional Airfoil with Ground Effect, Journal of Aircraft, Vol. 33, No. 2, March-April 1996, pp. 386-392.

[6] Kieffer, W., Moujaes, S. & Armbya, N., CFD Study of Section Characteristics of Formula Mazda Race Car Wings, Mathematical and Computer Modelling, Vol. 43, No. 11-12, June 2006, pp. 1275-1287.

[7] Mahon, S. & Zhang, X., Computational Analysis of Pressure and Wake Characteristics of an Aerofoil in Ground Effect, Journal of Fluids Engineering, Vol. 127, March 2005, pp. 290-298.

[8] Mokhtar, W.A., A Numerical Study of High-Lift Single Element Airfoils with Ground Effect for Racing Cars, Vehicle Aerodynamics 2005, Detroit, Michigan, April 11-14, 2005.

[9] Pinkerton, R. M., The Variation with Reynolds Number of Pressure Distribution Over an Airfoil Section, Technical Report, No. 613, N.A.C.A., 1938.

[10] Plotkin, A. & Dodbele, S.S., Slender Wing in Ground Effect, AIAA Journal, Vol.26, No.4, April 1988, pp. 493-494.

[11] Ranzenbach, R., Cambered Airfoil in Ground Effect – Wind Tunnel and Road Conditions, 13th AIAA Applied Aerodynamics Conference, San Diego, CA, USA, 19-22 June 1995, Technical Papers. Pt. 2, pp. 1208-1215.

[12] Suh, Y.B. & Ostowari, C., Drag Reduction Factor Due to Ground Effect, Journal of Aircraft, Vol. 25, No. 11, November 1988, pp. 1071-1072.

[13] Wright, P., Formula 1 Technology, Society of Automotive Engineers, Warrendale, USA, 2001.

[14] Zerihan, J., An Investigation into the Aerodynamics of Wings in Ground Effect, Ph.D. Thesis, University of Southampton, School of Engineering Sciences, April 2001.

[15] Katz, J., Race Car Aerodynamics: Designing for Speed, Bentley Publishers, Cambridge, USA, 1995.

[16] Zerihan, J. & Zhang, X., Aerodynamics of a Single Element Wing in Ground Effect, Journal of Aircraft, Vol. 37, No. 6, November-December 2000, pp. 1058-1064.

[17] Zhang, X. & Zerihan, J., Off-Surface Aerodynamic Measurements of a Wing in Ground Effect, Journal of Aircraft, Vol. 40, No. 4, July-August 2003, pp. 716-725.